



RESEARCH ARTICLE

Expansion Cooling in the Matrix Plume is Under-Recognized in MALDI Mass Spectrometry

Yong Jin Bae,¹ Jeong Hee Moon,² Myung Soo Kim¹¹Department of Chemistry, Seoul National University, Seoul 151–742, Korea²Medical Proteomics Research Center, KRIBB, Daejeon 305–806, Korea

Abstract

Time-of-flight (TOF) mass spectra for a peptide (Y_6) were obtained by utilizing matrix-assisted infrared laser desorption ionization (IR-MALDI) with glycerol as the matrix and by ultraviolet MALDI with α -cyano-4-hydroxycinnamic acid (CHCA), sinapinic acid (SA), and 2,5-dihydroxybenzoic acid (DHB). Collisional activation during ion extraction and exothermicity in the gas-phase proton transfer were found to be unimportant as the driving forces for in-source (ISD) and post-source (PSD) decays, indicating that the thermal energy acquired during photo-ablation is responsible for their occurrence. The temperatures of $[Y_6+H]^+$ in the 'early' and 'late' matrix plumes were estimated by the kinetic analysis of the ISD and PSD yields, respectively. The order of the temperatures was glycerol < DHB \approx SA < CHCA in the early plume and glycerol < DHB < SA < CHCA in the late plume. For each matrix, the temperature in the late plume was lower than in the early plume by 300–400 K, which was attributed to expansion cooling. The model (thermalization followed by expansion cooling) proposed to explain the occurrence of both rapid ISD and slow PSD is not only in sharp contrast with but also mutually exclusive with the prevailing explanation that the exothermicity in proton transfer and in-plume collisional activation are the driving forces for ion fragmentation in MALDI. The model also explains why MALDI is more successful for mass spectrometry of labile molecules than other desorption techniques that do not utilize a matrix. Factors affecting the plume temperature are also discussed.

Key words: MALDI, Plume temperature, Expansion cooling, Dissociation efficiency, Peptide dissociation, In-source decay, Post-source decay

Introduction

Matrix-assisted laser desorption ionization (MALDI) [1–5]/time-of-flight (TOF) mass spectrometry is useful for labile biological molecules. Dissociation of precursor ions generated by MALDI is also useful. Analysis of product ions formed inside (in-source decay, ISD, [6–8]) and outside (post-source decay, PSD, [9]) the source is useful for peptide

sequencing. Recently, ISD for peptides is attracting attention because of the formation of c and z type ions. This work, however, is focused on the formation of b and y ions to investigate the processes contributing to ion fragmentation in MALDI.

Even though ISD and PSD can be readily detected with modern MALDI-tandem TOF instruments employing delayed extraction and reflectron, the driving force(s) for their occurrence has not been established. Hillenkamp and Karas [1] listed collisional activation (CA) in the MALDI plume, direct excitation in the matrix crystal, and exothermicity in the ion formation process as possible driving forces. They are similar to the three mechanisms for PSD proposed by Spengler [9]; (A) direct photon-molecule interaction, temperature effect, and excess energy from

Electronic supplementary material The online version of this article (doi:10.1007/s13361-011-0115-y) contains supplementary material, which is available to authorized users.

Correspondence to: Myung Soo Kim; e-mail: myungsoo@snu.ac.kr

Received: 5 January 2011
Revised: 20 February 2011
Accepted: 23 February 2011
Published online: 9 April 2011

ionization, (B) low-energy multiple CA in the plume, and (C) post-source high-energy CA in the vacuum. Mechanism C can be ignored for instruments operating under very high vacuum. Spengler suggested that mechanism B would not be important in measurements with instruments utilizing delayed extraction. Direct photon-molecule interaction can also be ignored when the analyte is a poor absorber such as underivatized peptides in MALDI at 337 nm. Therefore, the temperature effect and excess energy from ionization are left as candidates. However, CA is still invoked in the prevailing explanation for ion fragmentation in MALDI [1]. For example, De Pauw et al. [8] mentioned the exothermicity in proton transfer as the driving force for ISD and CA during ion extraction as that for PSD.

Recently [10, 11], PSD and time-resolved photodissociation (PD) yields of $[Y_6+H]^+$ (Y =tyrosine) formed by UV-MALDI with α -cyano-4-hydroxycinnamic acid (CHCA), sinapinic acid (SA), and 2,5-dihydroxybenzoic acid (DHB) were analyzed and their temperature and dissociation rate constant ($k(E)$) were determined. A peptide ion temperature of 400–470 K thus obtained, with the internal energy distribution at a temperature assumed as Boltzmann, was in close agreement with those determined by Mowry and Johnston [12] through the photoionization of neutrals desorbed by MALDI. However, it was significantly lower than the 736–960 K estimated by Yergey et al. [13] from the ISD yield or the surface temperature (>800 K) reported by Zenobi et al. [14]. In our subsequent study [15], ISD of $[Y_6+H]^+$ was found to occur efficiently but subside rapidly. The observed ISD efficiency and lifetime indicated that $[Y_6+H]^+$ should have been absent in the MALDI-TOF spectra if the temperature at the time of ISD had persisted. The latter temperature estimated by analyzing the ISD yields with $k(E)$ was 800–870 K, close to those reported by Yergey et al. and Zenobi et al. The presence of two separate populations of $[Y_6+H]^+$ with widely different temperatures seemed unlikely because rapid thermalization would occur in the ‘early’ MALDI plume (>1 atm, reference [9]). As recognized previously [1, 3], a high-density early plume will undergo cooling via adiabatic expansion into a vacuum. Hence, the wide difference between the temperatures for ISD and PSD was considered as evidence that hot peptide ions in the early plume undergo expansion cooling. That is, the temperatures estimated from the ISD yields were those before expansion cooling (‘early’ plume) and, hence, were high and close to the surface temperature. In contrast, the temperatures measured by tandem mass spectrometry (PSD and PD) and by photoionization were those after expansion cooling (‘late’ plume) and, hence, were lower. The same was predicted in the computational study of DHB-MALDI by Knochenmuss and Zhigilei [16], with an early plume at 800 K cooling to about half that value. In a subsequent work [17], the temperatures in a CHCA plume were utilized for a dissociation kinetic study of peptide ions.

The above ISD study was done to find out why the temperature determined by tandem mass spectrometry was lower than previous rough estimates. After the study, we

realized that expansion cooling would have far-reaching significance in understanding MALDI-TOF of labile molecules and would require further testing, especially since the exothermicity/in-plume CA model is the prevailing explanation in the literature for ion fragmentation in MALDI. In this work, we obtained fragmentation data for $[Y_6+H]^+$ with IR-MALDI with glycerol and UV-MALDI with CHCA, SA, and DHB. We will show that the data are compatible with the thermalization/expansion cooling model but not with the exothermicity/in-plume CA model.

Experimental

Two MALDI-tandem TOF instruments were used; one for UV-MALDI and the other for IR-MALDI. As reported previously [18], the first instrument was comprised of an ion source with delayed extraction, a linear TOF analyzer, an ion gate, a PD cell, and a second-stage analyzer equipped with a reflectron with linear-plus-quadratic (LPQ) potential inside. Due to a deflection system [19] in the linear TOF region, only the product ions formed between its exit and the reflectron entrance (PSD region) were detected as PSD. The flight time of a precursor ion in the PSD region was 16.5% of its total flight time to the detector; 337 nm output from a nitrogen laser (MNL100, Lasertechnik Berlin, Berlin, Germany) focused by $f=250$ mm lens was used for MALDI.

Ion optical design of the IR-MALDI instrument (instrument 1 in reference [20]) was similar. A schematic drawing of its ion source is shown in Figure 1. Electrode layout and use of a 1.5 mm diameter hemispherical cavity on the sample plate for sample loading were the same as in a previous design [21] except that the cavity was not covered with a grid. The sample plate was cooled by cold ethanol from a thermostat (cc815 vpc, Huber, Offenburg, Germany).

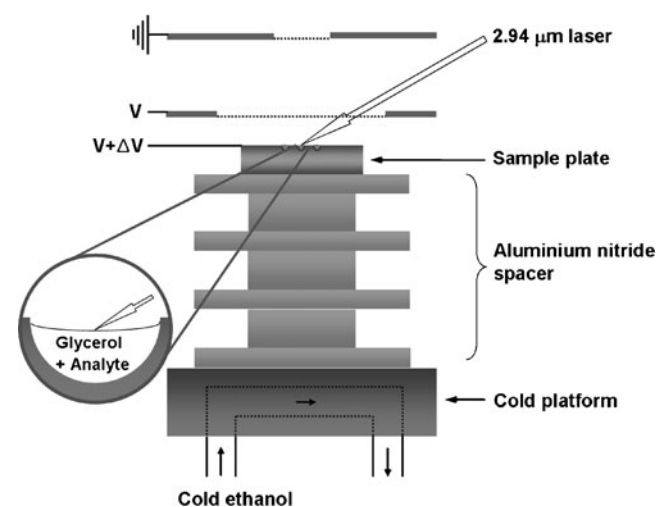


Figure 1. A schematic of the ion source in IR-MALDI-TOF instrument. Sample is loaded in a 1.5 mm diameter hemispherical cavity drilled on the sample plate, which is cooled by cold ethanol from a thermostat. 2.94 μ m OPO laser is used for MALDI

The sample plate temperature was $-15\text{ }^{\circ}\text{C}$, and the ion source pressure was 1×10^{-7} Torr. Even though the sample temperature affected the threshold laser pulse energy for MALDI, it did not affect the spectral data. A $2.94\text{ }\mu\text{m}$ OPO laser (IR Opolette 2731, Oportek, Carlsbad, CA, USA) focused by a CaF_2 lens ($f=105\text{ mm}$) was used. For mass calibration in PSD, the photodissociation spectrum was acquired by perpendicularly irradiating the lowest mass isotopomer ('A' peak) of a precursor ion with a 193 nm output of an excimer laser (PSX-100, MPB Communication, Montreal, Quebec, Canada). From a spectrum averaged over 3000 shots, ion abundances were evaluated as described previously [15, 17].

Peaks Appearing in a MALDI Spectrum

A precursor ion and its ISD products appear in a MALDI spectrum. As explained previously [17], however, PSD product ions, either from a precursor ion or from its ISD products, appear with good resolution in a MALDI spectrum obtained with an LPQ reflectron. For UV-MALDI in this work, abundances of product ions formed by ISD and PSD of a precursor ion and those by PSD of its ISD products were measured from the MALDI spectrum to ensure the same measurement conditions. For glycerol IR-MALDI, the PSD of the ISD products was too weak to measure.

Samples

YYYYYY (Y_6), CHCA, DHB, SA, glycerol, and other chemicals were purchased from Sigma (St. Louis, MO, USA). For UV-MALDI, a matrix solution prepared with 1:1 acetonitrile/0.1% trifluoroacetic acid was mixed with aqueous solution of Y_6 . For IR-MALDI, Y_6 was simply dissolved in glycerol. In both cases, matrix-to-analyte molar ratio was 1000:1.

Results

Spectra

Even though the UV-MALDI spectra of Y_6 with CHCA and DHB were reported previously [15, 17], they have been recorded again because of our decision to compare spectra obtained with 1.5 times the threshold pulse energy in all the cases. The spectra obtained with CHCA, SA, and DHB are shown in Figure 2a–c, respectively. Each spectrum was normalized to the precursor ion intensity. Prominent fragment ions formed by the ISD, PSD, and PSD of the ISD products are marked in the spectra, which are mostly a , b , y , and the immonium ion Y . The product ion abundance in UV-MALDI decreased in the order of $\text{CHCA} > \text{SA} > \text{DHB}$ in good agreement with their classification as 'hot,' 'intermediate,' and 'cold' matrices, respectively [22]. Among the

ISD product ions, only y_5 can be recognized in the glycerol IR-MALDI (Figure 2d). The weaker ISD than in the UV-MALDI is in good agreement with the consensus [5] that IR-MALDI is 'softer'.

The PSD spectra recorded by activating the ion gate are shown in Figure 3. The product ions in UV-MALDI-PSD of $[\text{Y}_6+\text{H}]^+$ were essentially the same as those formed by ISD. The product ion abundance order in PSD was the same as in ISD. In the IR-MALDI-PSD spectrum (Figure 3d), broad bands appeared at positions close to those for the product ion peaks in the UV-MALDI-PSD. A photodissociation (PD) spectrum at 193 nm was recorded for $[\text{Y}_6+\text{H}]^+$ generated by glycerol IR-MALDI for mass calibration. The b_4 peak in IR-MALDI-PD was compared with the same peak in UV-MALDI-PSD and IR-MALDI-PSD recorded with two different delay times—the time between MALDI laser irradiation and extraction field pulsing—in Figure 4. The average m/z values of the bands in IR-MALDI-PSD (Figure 4c and d) were a little larger, or their flight times were a little longer, than that in IR-MALDI-PD (Figure 4a). Broadening of the IR-MALDI-PSD band was more serious at smaller delay time. In contrast, the same peak in UV-MALDI-PSD (Figure 4b) was narrower and almost overlapped with the PD peak. Even though some structures were seen in the high m/z side of the UV-MALDI-PSD peak, they were mostly due to the PSD of higher m/z isotopomers, as marked in Figure 4b. We interpreted the broad bands in IR-MALDI-PSD as the PSD of $[\text{Y}_6+\text{H}]^+$ that has undergone collisional activation (CA), and retardation at the same time, during ion extraction by the delayed field, or CA-PSD. A good overlap between UV-MALDI-PSD and PD peaks means that CA-PSD is not important in UV-MALDI-PSD, i.e. the peaks are mostly non-CA-PSD. Partial overlap between IR-MALDI-PSD and PD peaks suggests that the non-CA-PSD component may also be present in this case, even though it is weak.

Threshold Laser Pulse Energy and Optimum Delay Time

In our early MALDI study of Y_6 with CHCA [15], only $[\text{Y}_6+\text{H}]^+$ was counted for threshold determination, resulting in a $1.1\text{ }\mu\text{J/pulse}$. When the ISD product ions were also counted in a subsequent study [17], the threshold decreased to $0.75\text{ }\mu\text{J/pulse}$. Use of the latter guideline in this work resulted in a 1.1 and $1.6\text{ }\mu\text{J/pulse}$ for UV-MALDI with SA and DHB, respectively, and $110\text{ }\mu\text{J/pulse}$ in IR-MALDI. In terms of fluence (pulse energy \div spot area), the difference between UV- and IR-MALDI thresholds would narrow by a factor of ten—spot areas for 337 nm and $2.94\text{ }\mu\text{m}$ lasers were roughly 0.015 and 0.15 mm^2 , respectively. The delay times resulting in the best spectral resolution were 250 , 300 , 400 , and 1700 ns with CHCA, SA, DHB, and glycerol, respectively. The thresholds and optimal delay times are listed in Table 1.

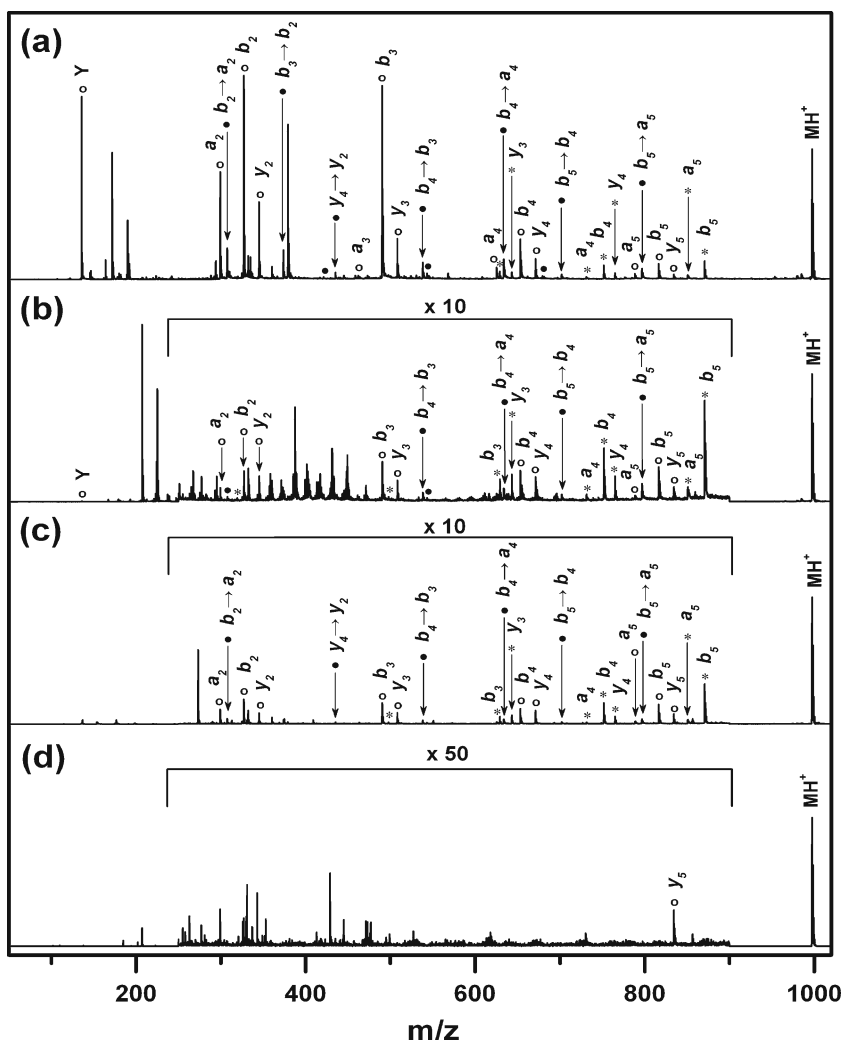


Figure 2. UV-MALDI spectra of Y_6 with (a) CHCA, (b) SA, and (c) DHB as matrices, and (d) glycerol IR-MALDI spectrum. Each spectrum was obtained with laser pulse energy corresponding to 1.5 times the threshold and normalized to the precursor ion peak height. Prominent fragment ions formed by ISD (open circle), PSD (*), and PSD of ISD products (filled circle) are marked. Other prominent peaks are due to matrices

Influence of MALDI Conditions on Product Ion Abundance

In our previous study of $[Y_6+H]^+$ [15] with CHCA and DHB, the sums of product ion abundances in ISD and PSD normalized to that of the precursor ion were called Y_{ISD} and Y_{PSD} , respectively. Both of these increased steadily with laser pulse energy, indicating an increase in the precursor ion internal energy. At a fixed laser pulse energy, Y_{ISD} was unaffected by the delay time (150–500 ns) along with Y_{PSD} , indicating that the ISD subsided rapidly. The same trends were observed for UV-MALDI with SA in this work (in the [Supplementary Material](#)).

In IR-MALDI, the glycerol-related peaks became very intense at a laser pulse energy corresponding to two times the threshold or larger. This led us to collect abundance data at 1.5 times the threshold for all the laser-matrix combinations in this work. As shown in the [Supplementary Material](#),

Y_{ISD} (abundance of y_5) was insensitive to the laser pulse energy, unlike in UV-MALDI. The precursor ion and y_5 peak regions in the IR-MALDI spectra recorded with four different delay times are shown in Figure 5. Tails appear at the high m/z sides of the precursor ion and y_5 peaks as the delay time got shorter. Regardless, Y_{ISD} was unaffected by the delay time, as shown in the [Supplementary Material](#). That is, ISD seems to subside rapidly, as in UV-MALDI, even though collisions during ion extraction deteriorate the resolution.

Product Ion Yields and Survival Probabilities

Even though post-source dissociation occurs over the entire region between the source exit and the detector, only the product ions formed in the PSD region are detected as PSD in our apparatus. In our dissociation kinetics study of peptide ions with CHCA [17], the total PSD yield, or $Y_{\text{total PSD}}$, was

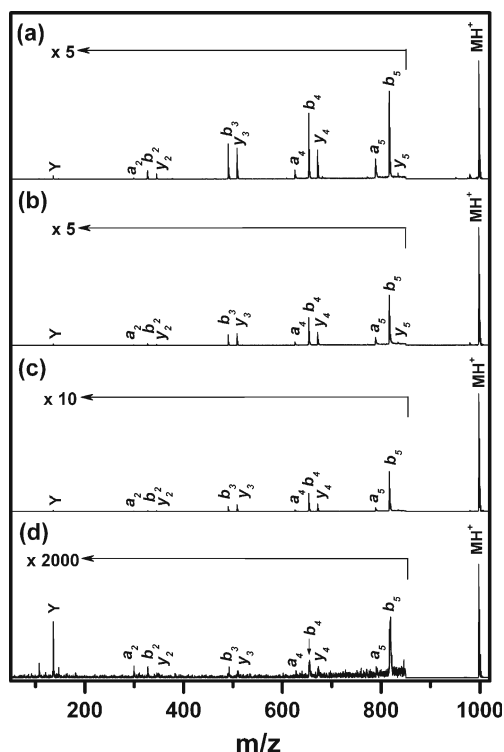


Figure 3. PSD spectra of $[Y_6+H]^+$ formed by UV-MALDI with (a) CHCA, (b) SA, and (c) DHB as matrices, and by (d) glycerol IR-MALDI. Each spectrum was obtained with laser pulse energy corresponding to 1.5 times the threshold and normalized to the precursor ion peak height

roughly estimated as $6 \times Y_{\text{PSD}}$ because the flight time through the PSD region was $1/6$ of the total flight time. Then, the precursor ion abundance at the source exit became $1 + 6 \times Y_{\text{PSD}}$. A similar correction was made for each ISD product ion. Then, the total ISD yield, $Y_{\text{total ISD}}$, was evaluated by dividing the sum of the corrected abundances of ISD product ions by that of the precursor ion. Product ion yields in UV-MALDI with CHCA, SA, and DHB obtained in this work are listed in Table 2. Even though ISD product ions were more intense in the UV-MALDI spectrum with SA than with DHB, their $Y_{\text{total ISD}}$ values were similar. This occurred because $Y_{\text{total PSD}}$ was larger with SA and, hence, the denominator used in the estimation of $Y_{\text{total ISD}}$ was larger. This cautions against using uncorrected ion abundances as a relative measure of the matrix temperature. It is interesting to note that SA was hotter than DHB in PSD while the two matrices were comparable in ISD. $Y_{\text{total PSD}}$ in IR-MALDI-PSD was evaluated from the abundance of non-CA-PSD component extracted from each broad band (see Figure 4c). $Y_{\text{total PSD}}$ and $Y_{\text{total ISD}}$ thus obtained will be upper limits because of the potential contamination by collisional activation.

The survival probabilities of the precursor ion inside (S_{in}) and outside (S_{post}) the ion source are related to $Y_{\text{total ISD}}$ and $Y_{\text{total PSD}}$ by $1/(1+Y_{\text{total ISD}})$ and $1/(1+Y_{\text{total PSD}})$, respectively [17]. S_{in} and S_{post} thus obtained are also listed in Table 2.

Effective Temperatures

The effective temperatures of $[Y_6+H]^+$ in the early and late matrix plumes were estimated by a method previously reported [17] (shown in the Supplementary Material). Briefly, 50 ns was postulated as the lifetime of the ISD, or $1.4 \times 10^7 \text{ s}^{-1}$ as a rate constant which, in turn, corresponds to an internal energy of 11.585 eV for $k(E)$ determined by time-resolved photodissociation [11]. Then, the temperature in the early plume was determined such that the area below this energy in the internal energy distribution becomes S_{in} . Similarly, the temperature in the late plume was determined by analyzing S_{post} with $k=5.4 \times 10^4 \text{ s}^{-1}$ as the threshold rate constant. From S_{in} data obtained in this work, 874, 790, 788, and ≤ 721 K were estimated as the temperatures in the early CHCA, SA, DHB, and glycerol plumes, respectively. Those in the late plumes estimated from S_{post} were 461, 443, 423, and ≤ 347 K, respectively. The temperature data obtained in this work were close to but a little different from previous

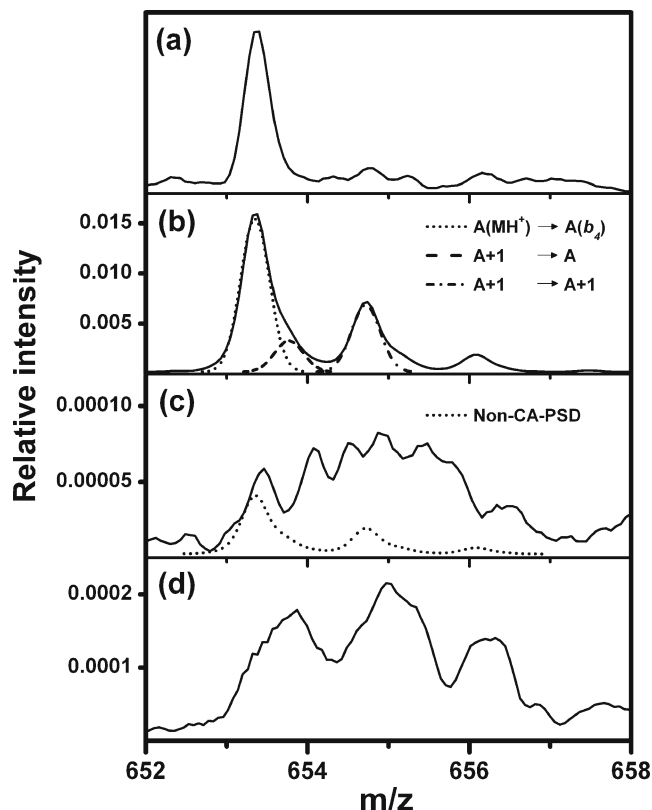


Figure 4. Shapes of b_4 peak recorded by (a) IR-MALDI-PD, (b) UV-MALDI-PSD with DHB, and IR-MALDI-PSD with (c) 1.75 μs , and (d) 1.15 μs delay time. Spectra (b)–(d) are normalized to the precursor ion peak height. In (a), only the lowest m/z isotopomer, or the A peak, of b_4 appears because only the A peak of $[Y_6+H]^+$ was selected for PD. Various isotopomeric peaks appear in PSD spectra. Some of them are resolved in (b) such as the dissociation of A of $[Y_6+H]^+$ to A of b_4 , etc. Non-CA-PSD component in each broad band in IR-MALDI-PSD was extracted by utilizing the corresponding shape in UV-MALDI-PSD, as shown in (c)

Table 1. Some Properties and MALDI Parameters for Matrices

	Proton affinity ^a (kJ mol ⁻¹)	Melting point (K)	Absorption coefficient ^b (10 ⁴ cm ⁻¹)	Threshold laser energy ^c (μJ/pulse)	Optimal delay time ^c (ns)
CHCA	766-933	518-523	21.8	0.75±0.08	250±50
SA	878-895	476-478	11.0	1.1±0.1	300±50
DHB	850-856	473-478	7.95	1.6±0.2	400±50
Glycerol	874	291	0.65	110±11	1700±100

^aData for CHCA, SA, and DHB are from ref. 4. That for glycerol is from ref. 29.

^bThose for CHCA, SA, and DHB are at 337 nm from ref. 30. That for glycerol is at 2.94 μm from ref. 31.

^cMeasured in this work for UV-MALDI at 337 nm and IR-MALDI at 2.94 μm

reports [11, 17] because the laser pulse energies used were different (two times the threshold in the previous studies versus 1.5 times the threshold in the present one) and/or the details of the method used to estimate the total post-source dissociation were different.

To estimate systematic errors in the temperature estimation, we changed parameters such as the $\times 6$ factor used to estimate the $Y_{\text{total PSD}}$. Their influence was not important. The most critical source of error was $k(E)$. In this work, we used the $k(E)$ determined previously [11]—specified by the critical energy of 0.60 eV and by the critical entropy of -28.4 eu (1 eu = 4.184 J K⁻¹ mol⁻¹). We also analyzed the data using substantially different $k(E)$ s even if they were incompatible with the PD rate constants measured previously. For example, $k(E)$ calculated using 0.90 eV and -14.2 eu—in the [Supplementary Material](#)—resulted in 939, 850, 848, and ≤ 777 K as the temperatures in the early plumes of CHCA, SA, DHB, and glycerol, respectively, and 634, 612, 589, and ≤ 494 K in the late plumes. It is evident that errors in temperature due to $k(E)$ can be significant. However, the order of temperature CHCA > SA \approx DHB > glycerol and CHCA > SA > DHB > glycerol in the early and late plumes, respectively, remained the same. More importantly, a substantial temperature drop in the late plume is seen regardless of the accuracy of $k(E)$.

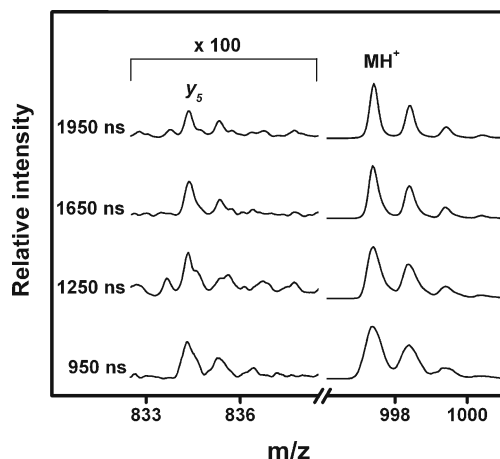


Figure 5. The precursor ion and y_5 peak regions in IR-MALDI spectra recorded with four different delay times. Laser energy corresponding to 1.5 times the threshold was used

Discussion

Collisional Activation (CA) as the Driving Force for PSD and ISD

Since IR penetrates the matrix deeper than UV and ablates at least 10 times more material [1, 23], a longer delay time is used in IR-MALDI to minimize the collisional deterioration of the resolution. Even then, we observed broad bands in the PSD due to the CA-PSD. However, such broad bands were extremely weak and difficult to mass-calibrate. That is, IR-MALDI-PSD is not a useful tandem mass spectrometric technique. Near absence of such bands in UV-MALDI-PSD (Figure 4b) means that CA during ion extraction is not important there.

With a short delay time in IR-MALDI, the peak shapes for $[Y_6+H]^+$ and y_5 deteriorated due to collisions during ion extraction. Regardless, $Y_{\text{total ISD}}$ remained the same. In addition, in spite of the higher plume density in IR-MALDI, the $Y_{\text{total ISD}}$ was much smaller than in UV-MALDI. These eliminate in-plume CA as a driving force for ISD. Even though the thermal energy exchange between an analyte and hot matrix molecules in the very early plume may contribute to ISD, we would rather call it thermalization because CA in tandem mass spectrometry usually means translational-to-internal energy conversion.

Exothermicity in Gas-Phase Proton Transfer as the Driving Force for ISD

The ΔH in proton transfer between a protonated matrix and an analyte is related to the proton affinities (PA) of neutral species by $PA(\text{matrix}) - PA(\text{analyte})$. If the heat released ($-\Delta H$) is the driving force for ion fragmentation as widely suggested [1, 8, 9, 24], a matrix with smaller PA will be hotter, i.e., induce more fragmentation. PA data from the literature for the matrices used are listed in Table 1. In testing this model, CHCA was not useful because its PA data are widely scattered. The average PA s for SA and DHB are 887 and 853 kJ mol⁻¹, respectively. The PA data predicted the order the temperature as SA < glycerol < DHB, in disagreement with the order found in this work, i.e., glycerol < DHB \leq SA.

Even though the exothermicity model has been popular, there was no estimation of the heat release in the proton transfer. Literature data [25] for the PA of glycine (G) and tyrosine (Y) are 881 and 924 kJ mol⁻¹, respectively. Change

Table 2. Product Ion Yields and Survival Probabilities for $[Y_6+H]^+$ and its Temperatures in Early (T_{early}) and Late (T_{late}) Matrix Plumes

	CHCA	SA	DHB	Glycerol
$Y_{\text{total ISD}}$	3.2 ± 0.1	0.20 ± 0.06	0.19 ± 0.02	≤ 0.006
$Y_{\text{total PSD}}$	4.5 ± 0.2	1.9 ± 0.3	0.68 ± 0.08	≤ 0.005
S_{in}	0.24 ± 0.01	0.83 ± 0.04	0.84 ± 0.02	≥ 0.994
S_{post}	0.18 ± 0.01	0.35 ± 0.06	0.60 ± 0.04	≥ 0.995
$T_{\text{early}}^a, \text{ K}$	874 ± 1	790 ± 7	788 ± 3	≤ 721
$T_{\text{late}}^a, \text{ K}$	$461 \pm 1(469)$	$443 \pm 3(445)$	$423 \pm 2(396)$	≤ 347

^aResults from the time-resolved photodissociation study [11] are in parentheses

in *PA* with respect to peptide size may parallel that of gas-phase basicity (*GB*). Since the *GB* of G_6 is larger than that of G by 78 kJ mol^{-1} [25], the *PA* of Y_6 may be around 1002 kJ mol^{-1} . Then, taking SA as an example, the heat release in the proton transfer would be around 115 kJ mol^{-1} , which will be shared by $[Y_6+H]^+$ and SA. Even the upper limit of energy that $[Y_6+H]^+$ can acquire looks too small to induce ISD on a nanosecond time scale—photo-excitation at 266 and 193 nm (450 and 620 kJ mol^{-1} , respectively) induced such a fast dissociation (60–110 ns) [10]. As a rough estimation of the temperature change that might possibly arise from the proton transfer, we added a half of the 115 kJ mol^{-1} to the energy at 445 K determined previously [11] and obtained 482 K. Compared with 790 K in the early plume determined in this work, 482 K looks too low to regard exothermicity as the main driving force for ISD.

Thermal Origin for ISD and PSD

From a kinetics perspective, an intriguing observation in MALDI is that some molecular ions arrive at the detector or dissociate slowly (PSD, on a $10 \mu\text{s}$ time scale) in spite of the rapid occurrence of ISD (on a 50 ns time scale). Even though different driving forces for ISD and PSD, e.g., exothermicity in proton transfer versus CA, might be an explanation, they have been invalidated in this work. This leaves the thermal energy gained during photo-ablation as the driving force for ion fragmentation. Heating of an analyte may start in the condensed phase and continue in the dense early plume, resulting in its thermalization. Then, the occurrence of both fast ISD and slow PSD can be reconciled if the thermal internal energy has a very broad distribution. However, we found [15, 17], shown in the [Supplementary Material](#), that the calculated distributions were not broad enough to accommodate a factor of a 200 difference in the rate constant. In addition, if the distribution were very broad, ISD would increase with delay time, against our observation. Hence, to explain the occurrence of both ISD and PSD, one must accept that the temperature of a peptide ion drops spontaneously as the plume expands. In fact, the occurrence of expansion cooling was acknowledged from supersonic ‘initial’ ion speeds [26] and was proposed to stabilize labile analyte ions [1, 3]. Expansion cooling and in-plume CA are mutually exclusive, i.e., internal-to-trans-

lational versus translational-to-internal energy conversions. In addition, a peptide ion somewhat hotter than its neighbors upon its formation will equilibrate if thermalization is efficient in the early plume. That is, the exothermicity/in-plume CA model is incompatible with thermalization/expansion cooling. Regardless, the former model still prevails in the literature [1, 8], probably because there has been no information on the extent of expansion cooling. Through kinetic analysis, we have shown that the peptide ion temperature drops significantly upon plume expansion, which, we believe, is one of the key characteristics of MALDI in the mass spectrometry of labile molecules.

Factors Affecting Plume Temperature

A question still outstanding is what determines the plume temperature. Hillenkamp and Karas [1] proposed to classify matrices as ‘hard’ or ‘soft’ rather than ‘hot’ or ‘cold’ with a connotation that a hard matrix will require more energy for ablation and, hence, generate hotter plume. As a rough measure of hardness, the matrix melting points are listed in Table 1—reliable data for matrix sublimation temperature and enthalpy are unavailable, even though they may be better measures of the mechanical hardness of a crystal. They predict the order of the temperature as glycerol < DHB \approx SA < CHCA, which is in fair agreement with the present results (the same order in the early plume and glycerol < DHB < SA < CHCA in the late plume). However, crystal hardness will not be the only factor affecting the plume temperature considering that IR-MALDI is invariably softer than UV-MALDI, even when the same matrix is used for both [27]. Hillenkamp and Karas noted that hard matrices correlated with low initial ion speeds. Based on the initial speed data reported by Glückmann and Karas [28] and by Berkenkamp et al. [26], the order of hardness becomes glycerol < DHB < SA < CHCA. The same order holds for the absorption coefficient (Table 1) and the opposite for the threshold energy and optimal delay time. All of these may be explained as follows. With a smaller matrix absorption coefficient, the laser penetrates deeper, requiring larger energy for ablation. This results in larger amount of materials ablated and, hence, a higher plume pressure. The latter not only necessitates longer delay time but also causes a more severe temperature drop, resulting in

less ion fragmentation. That is, in addition to the mechanical hardness of a matrix crystal, its absorption coefficient may affect the plume temperature by controlling the amount of materials ablated and, hence, the extent of expansion cooling. For example, even though DHB is as hot as SA in the early plume, it is cooler in the late plume, possibly due to its smaller absorption coefficient.

To summarize, the order of the temperature found in this work seems to be consistent with the concept of matrix hardness proposed by Hillenkamp and Karas. However, further study is needed to find out whether mechanical hardness and absorption coefficient are the main factors determining plume temperature and how their combined effect operates.

References [29–31] are cited in Table 1.

Conclusion

It is well established that a very hot early plume is formed in MALDI and that rapid dissociation of protonated species of labile molecules such as peptides and proteins occurs in the early plume. In this regard, the fact that intact molecular ion peaks appear in MALDI-TOF spectra is very intriguing. The model presented in this work, i.e., expansion cooling in the matrix plume, provides an explanation for this curious phenomenon. The model also provides an explanation for the fact that labile species are more difficult to detect when a matrix is not used such as in laser desorption and secondary ion mass spectrometry. There, hot labile species generated in the gas phase might dissociate and, hence, become undetectable. In this regard, expansion cooling in the matrix plume is one of the key characteristics of MALDI, which has not received as much attention as it deserves.

The early plume formed by MALDI may not be as physically homogenous as assumed in this work. For example, the characteristics of the plume formed by ablation of the top layer of a sample may be somewhat different from those formed from within deeper layers. In addition, operational efforts to optimize each MALDI experiment may result in sampling different portions of a possibly heterogeneous plume. Such variability was ignored in this work. It should be mentioned that details of the processes of material ablation and ion formation in MALDI are subjects of active investigation. A better understanding of such processes will certainly provide better insights on ion fragmentation. We hope that the occurrence of expansion cooling in the matrix plume and its extent found in this work prove useful in the effort to elucidate the mysteries surrounding MALDI.

Acknowledgments

The authors acknowledge financial supported for this by the National Research Foundation, Republic of Korea. Y.J.B. thanks the Ministry of Education, Science, and Technology, Republic of Korea, for Brain Korea 21 Fellowship.

References

1. Hillenkamp, F., Karas, M.: The MALDI Process and Method. In: Hillenkamp, F., Peter-Katalinić, J. (eds.) MALDI MS. A Practical Guide to Instrumentation, Methods and Applications, pp. 1–28. Wiley-VCH, Weinheim (2007)
2. Zenobi, R., Knochenmuss, R.: Ion Formation in MALDI Mass Spectrometry. *Mass Spectrom. Rev.* **17**, 337–366 (1998)
3. Dreisewerd, K.: The Desorption Process in MALDI. *Chem. Rev.* **103**, 395–425 (2003)
4. Knochenmuss, R.: Ion Formation Mechanisms in UV-MALDI. *Analyst* **131**, 966–986 (2006)
5. Dreisewerd, K., Berkenkamp, S., Leisner, A., Rohlfling, A., Menzel, C.: Fundamentals of Matrix-Assisted Laser Desorption/Ionization Mass Spectrometry with Pulsed Infrared Lasers. *Int. J. Mass Spectrom.* **226**, 189–209 (2003)
6. Brown, R.S., Carr, B.L., Lennon, J.J.: Factors That Influence the Observed Fast Fragmentation of Peptides in Matrix-Assisted Laser Desorption. *J. Am. Soc. Mass Spectrom.* **7**, 225–232 (1996)
7. Köcher, T., Engström, Å., Zubarev, R.A.: Fragmentation of Peptides in MALDI In-Source Decay Mediated by Hydrogen Radicals. *Anal. Chem.* **77**, 172–177 (2005)
8. Demeure, K., Gabelica, V., De Pauw, E.A.: New Advances in the Understanding of the In-Source Decay Fragmentation of Peptides in MALDI-TOF-MS. *J. Am. Soc. Mass Spectrom.* **21**, 1906–1917 (2010)
9. Spengler, B.: Post-Source Decay Analysis in Matrix-Assisted Laser Desorption/Ionization Mass Spectrometry of Biomolecules. *J. Mass Spectrom.* **32**, 1019–1036 (1997)
10. Moon, J.H., Yoon, S.H.: Kim, M. S. Temperature of Peptide Ions Generated by Matrix-Assisted Laser Desorption Ionization and Their Dissociation Kinetic Parameters. *J. Phys. Chem. B* **113**, 2071–2076 (2009)
11. Yoon, S.H., Moon, J.H., Kim, M.S.: Time-Resolved Photodissociation Study of Singly Protonated Peptides with a Histidine Residue Generated by Matrix-Assisted Laser Desorption Ionization: Dissociation Rate Constant and Internal Temperature. *J. Am. Soc. Mass Spectrom.* **20**, 1522–1529 (2009)
12. Mowry, C.D., Johnston, M.V.: Internal Energy of Neutral Molecules Ejected by Matrix-Assisted Laser Desorption. *J. Phys. Chem.* **98**, 1904–1909 (1994)
13. Campbell, J.M., Vestal, M.L., Blank, P.S., Stein, S.E., Epstein, J.A., Yergey, A.L.: Fragmentation of Leucine Enkephalin as a Function of Laser Fluence in a MALDI TOF-TOF. *J. Am. Soc. Mass Spectrom.* **18**, 607–616 (2007)
14. Koubenakis, A., Frankevich, V., Zhang, J., Zenobi, R.: Time-Resolved Surface Temperature Measurement of MALDI Matrices Under Pulsed UV Laser Irradiation. *J. Phys. Chem. A* **108**, 2405–2410 (2004)
15. Yoon, S.H., Moon, J.H., Kim, M.S.: A Comparative Study of In- and Post-Source Decays of Peptide and Preformed Ions in Matrix-Assisted Laser Desorption Ionization Time-of-Flight Mass Spectrometry: Effective Temperature and Matrix Effect. *J. Am. Soc. Mass Spectrom.* **21**, 1876–1883 (2010)
16. Knochenmuss, R., Zhigilei, L.V.: Molecular Dynamics Simulations of MALDI: Laser Fluence and Pulse Width Dependence of Plume Characteristics and Consequences for Matrix and Analyte Ionization. *J. Mass Spectrom.* **45**, 333–346 (2010)
17. Yoon, S.H., Moon, J.H., Kim, M.S.: Changes in Dissociation Efficiency and Kinetics of Peptide Ions Induced by Basic Residues and Their Mechanistic Implication. *J. Am. Soc. Mass Spectrom.* **22**, 214–220 (2011)
18. Moon, J.H., Yoon, S.H., Kim, M.S.: Construction of an Improved Tandem Time-of-Flight Mass Spectrometer for Photodissociation of Ions Generated by Matrix-Assisted Laser Desorption Ionization (MALDI). *Bull. Korean Chem. Soc.* **26**, 763–768 (2005)
19. Yoon, S.H., Moon, J.H., Choi, K.M., Kim, M.S.: A Deflection System to Reduce the Interference from Post-Source Decay Product Ions in Photodissociation Tandem Time-of-Flight Mass Spectrometry. *Rapid Commun. Mass Spectrom.* **20**, 2201–2208 (2006)
20. Bae, Y.J., Yoon, S.H., Moon, J.H., Kim, M.S.: Optimization of Reflector for Kinetic and Mechanistic Studies with Multiplexed Multiple Tandem (MSⁿ) Time-of-Flight Mass Spectrometry. *Bull. Korean Chem. Soc.* **31**, 92–99 (2010)
21. Cha, H.J., Moon, J.H., Kim, M.S.: Resolution of Infrared Matrix-Assisted Laser Desorption/Ionization Time-of-Flight Mass Spectrometry

- try Using Glycerol; Enhancement with a Disperse Laser Beam. *Rapid Commun. Mass Spectrom.* **21**, 1468–1474 (2007)
22. Gabelica, V., Schulz, E., Karas, M.: Internal Energy Build-up in Matrix-Assisted Laser Desorption/Ionization. *J. Mass Spectrom.* **39**, 579–593 (2004)
 23. Kampmeier, J., Dreisewerd, K., Schürenberg, M., Strupat, K.: Investigation of 2,5-DHB and Succinic Acid as Matrices for IR and UV MALDI. Part I: UV and IR Laser Ablation in the MALDI Process. *Int. J. Mass Spectrom. Ion Processes* **169/170**, 31–41 (1997)
 24. Stevenson, E., Breuker, K., Zenobi, R.: Internal Energies of Analyte Ions Generated from Different Matrix-Assisted Laser Desorption/Ionization Matrices. *J. Mass Spectrom.* **35**, 1035–1041 (2000)
 25. Harrison, A.G.: The Gas-Phase Basicities and Proton Affinities of Amino Acids and Peptides. *Mass Spectrom. Rev.* **16**, 201–217 (1997)
 26. Berkenkamp, S., Menzel, C., Hillenkamp, F., Dreisewerd, K.: Measurements of Mean Initial Velocities of Analyte and Matrix Ions in Infrared Matrix-Assisted Laser Desorption Ionization Mass Spectrometry. *J. Am. Soc. Mass Spectrom.* **13**, 209–220 (2002)
 27. Strupat, K., Kampmeier, J., Horneffer, V.: Investigations of 2,5-DHB and Succinic Acid as Matrices for UV and IR MALDI. Part II: Crystallographic and Mass Spectrometric Analysis. *Int. J. Mass Spectrom. Ion Processes* **169/170**, 43–50 (1997)
 28. Glückmann, M., Karas, M.: The Initial Ion Velocity and Its Dependence on Matrix, Analyte and Preparation Method in Ultraviolet Matrix-Assisted Laser Desorption/Ionization. *J. Mass Spectrom.* **34**, 467–477 (1999)
 29. Sunner, J.A., Kulatunga, R., Kebarle, P.: Fast Atom Bombardment Mass Spectrometry and Gas-Phase Basicities. *Anal. Chem.* **58**, 1312–1316 (1986)
 30. Allwood, D.A., Dreyfus, R.W., Perera, I.K., Dyer, P.E.: UV Optical Absorption of Matrices Used for Matrix-Assisted Laser Desorption/Ionization. *Rapid Commun. Mass Spectrom.* **10**, 1575–1578 (1996)
 31. Fan, X., Little, M.W., Murray, K.K.: Infrared Laser Wavelength Dependence of Particles Ablated from Glycerol. *Appl. Surf. Sci.* **255**, 1699–1704 (2008)